

http://pubs.acs.org/journal/aesccq Article

Evolution of Sea Spray Aerosol Particle Phase State Across a Phytoplankton Bloom

Paul R. Tumminello, Reece C. James, Samantha Kruse, Allison Kawasaki, Adam Cooper, Isis Guadalupe-Diaz, Karen Lopo Zepeda, Daniel R. Crocker, Kathryn J. Mayer, Jonathan S. Sauer, Christopher Lee, Kimberly A. Prather, and Jonathan H. Slade*



Cite This: https://doi.org/10.1021/acsearthspacechem.1c00186



ACCESS

Metrics & More

Article Recommendations

Supporting Information

ABSTRACT: Sea spray aerosol (SSA) represents the largest flux of aerosol mass annually, impacting Earth's climate and the hydrological cycle by acting as cloud condensation and ice nuclei. The phase state (viscosity, η) of aerosol particles is important for aerosol impacts on climate and air quality, but the viscosity of SSA and chemical and biological drivers have not been evaluated. We measured variability in the relative humidity (RH)-dependent phase states of SSA (with a peak number-weighted aerodynamic diameter of \sim 0.2 μ m) based on



particle bounce factors (BFs) and calculated glass transition temperatures and η of the organic components in SSA ($\eta_{\rm org}$) from online molecular composition measurements during an induced phytoplankton bloom. The results demonstrate that the SSA BFs and $\eta_{\rm org}$ vary throughout the bloom, with the bulk of the SSA number concentration as liquidlike below the deliquescence and efflorescence RH of sea salt prior to phytoplankton growth on the basis of a measured BF of \leq 0.2 and an estimated $\eta_{\rm org}$ of <10² Pa·s. In contrast, the organic components in SSA exhibit viscous semisolid-like phase states over the same RH range during the peak of phytoplankton growth (BF~0.8 and estimated $\eta_{\rm org}$ ~10³ Pa·s). Including the η of the aqueous inorganic salt, under the assumption that it is internally and homogeneously mixed with the organic components, significantly reduces the estimated η of the SSA mixture. The differences in SSA phase state across the bloom appear to be partially driven by specific biological processes in the seawater that alter the average molecular properties of the organic compounds in SSA (e.g., molar mass and hygroscopicity) depending upon the stage of the phytoplankton bloom. These findings have implications for aerosol processing, particularly in the biologically active coastal marine environment, including potential influences on ice nucleation and gas—particle partitioning.

KEYWORDS: sea spray aerosol, phase state, glass transition, viscosity, bounce, phytoplankton bloom, mass spectrometry

1. INTRODUCTION

Sea spray aerosol (SSA) constitutes the largest flux of naturally produced particles by mass annually. SSA impacts climate directly by scattering solar radiation² and indirectly by serving as cloud condensation nuclei (CCN)³ and ice nuclei (IN). SSA consists of internally and externally mixed inorganic (sea salt) and organic material derived from components at the sea surface that selectively partition to aerosol when waves break and bubbles collapse. 5,6 The chemical composition of SSA is highly dependent on the biological activity of seawater and varies with particle size, with 45–85% of the submicron SSA number concentration containing organic carbon when chlorophyll a (Chl-A) concentrations peak,8 a proxy for phytoplankton primary productivity. The organic compounds in SSA are largely composed of free saccharides, polysaccharides, and short- and long-chain fatty acids, which have been shown to influence SSA physicochemical properties (e.g., hygroscopicity). 2,9,10

In addition to its effects on aerosol hygroscopicity, the chemical identity of the organic material can affect the aerosol phase state (viscosity). The phase state can in turn impact

the CCN activity,¹⁴ IN efficiency,⁴ and gas—particle interactions,¹⁵ including heterogeneous reactivity¹⁶ and the lifetimes of toxic substances in the aerosol phase.¹⁷ Although the oceans represent a significant and continuous flux of particulate mass to the atmosphere,¹⁸ and particles can exist with a multitude of phase states across the atmosphere,¹⁹ the phase states of SSA have largely been unstudied and not included in the global modeled atmosphere. Only a few studies have characterized, offline, the phase states and morphologies of nascent SSA particles.^{20–22} Currently, the molecular and biological drivers of SSA phase state and the time scales over which it might change during a phytoplankton bloom are poorly understood. Better temporal resolution in the measured

Special Issue: Mario Molina Memorial

Received: June 4, 2021 Revised: September 22, 2021 Accepted: September 28, 2021



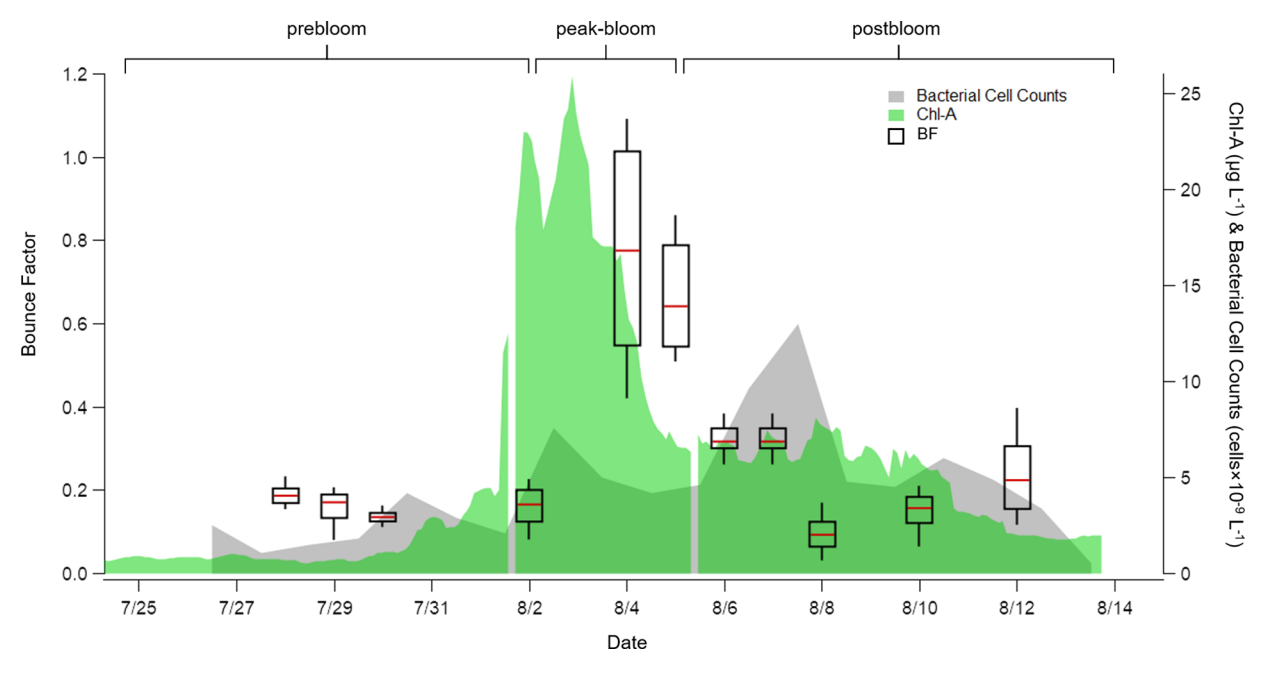


Figure 1. (A) Daily bounce factors measured at \sim 50% RH and shown as box plots, where the red line indicates the median BF, the 75th percentiles are bounded by the boxes, and the 95th percentiles are represented by the whiskers. Concentrations of chlorophyll-A (Chl-A, green) and bacterial cell counts (gray) are also shown. For each day of the study there were approximately >60 BF data points at a given RH. The bloom is divided into three segments as described in the main text and labeled at the top of the figure.

phase state of SSA is needed to account for the rapid compositional changes that SSA experiences when biological activity in the water and ambient relative humidity (RH) change following ejection from the ocean surface. Herein we report the transient and evolving phase states and molecular composition of nascent SSA online over the course of a phytoplankton bloom and as a function of RH in a controlled wave flume experiment as part of the 2019 National Science Foundation—Center for Aerosol Impacts on Chemistry of the Environment (NSF-CAICE) SeaSCAPE (Sea Spray Chemistry and Particle Evolution) experiment. Evolution

2. RESULTS AND DISCUSSION

2.1. SSA Particle Bounce as a Function of Biological **Activity.** The phase state of SSA was evaluated in real time during the phytoplankton bloom on the basis of particle bounce measurements and reported here as a bounce factor (BF) (see sections 4.1-4.3 for more details). An illustration of the setup is provided in Figure S1. Representative normalized size distributions of solidlike polydisperse ammonium sulfate aerosol generated in the laboratory and measured by an electrical low-pressure impactor (ELPI+) (Dekati Ltd.) with smooth Al-foil plates and combined scanning electrical mobility sizer (SEMS) (Brechtel) and aerodynamic particle sizer (APS) (TSI Inc.) are shown in Figure S2, demonstrating that when particles bounce the size distribution is skewed toward smaller size bins. Comparisons between the BF method applied here (without size selection) and other studies in Table S1 show very good agreement using different test liquids and solid aerosols under similar experimental conditions. In Figure 1, the BF of the nascent "primary" SSA, including all sizes in the detectable range (aerodynamic diameters between ~0.01 and \sim 6 μ m; see Figure S2), is shown between July 28 and August 12 over the life cycle of an induced phytoplankton bloom. The life cycle of the bloom was evaluated by monitoring the concentration of Chl-A (green) and bacteria

cell counts (gray); the latter indicates the onset of phytoplankton decay. For simplicity, the bloom can be categorized into three segments: prebloom, peak-bloom, and postbloom, as indicated along the top of Figure 1.24 Here we have plotted the median and quartile BFs for each day of the study measured at ~50% RH. During the prebloom phase (July 28-August 2), BF median values were relatively low between ~ 0.1 and ~ 0.2 , indicative of liquidlike or low-viscosity semisolid particles.²⁵ This stage of the bloom is characterized by low biological activity given the relatively low Chl-A and bacterial cell counts. During the peak bloom phase (August 2– 5), we observed a significant increase in median BF up to \sim 0.8 at ~50% RH, indicative of highly viscous phase states of SSA particles in which most of the particles that were sampled bounced. We note that the missing data on July 31, August 1, and August 3 resulted from instrument maintenance, and therefore, we could not extrapolate how the BF evolved on those days. As the phytoplankton concentration decreased during the postbloom phase (August 5-12), the BF also decreased. Observations on August 9 and 11 are not included because the conditions of the wave flume were altered on those days. The maximum BF during peak Chl-A, minimum BF during the prebloom stage, and decrease in BF during postbloom were generally consistent with an independent mesocosm study using a marine aerosol reference tank (MART), 26,27 which we conducted prior to SeaSCAPE using seawater collected from the same location (Figure S3).

2.2. Relative Humidity Dependence of SSA Particle Bounce. The changes in BF during the phytoplankton bloom indicate transitions between liquid and solidlike SSA particles that are dependent on the stage of the phytoplankton bloom and total biomass in the seawater. Because water can act as a plasticizer to decrease the viscosity of aerosol at high RH, $^{12,16,28-30}$ we examined the effects of varying RH on the SSA phase state by systematically varying the sample RH from \sim 75% to \sim 20%, covering a wide range of relevant atmospheric

RH as well as the deliquescence RH (DRH) (~75%) and efflorescence RH (ERH) (~44%) of NaCl.³¹ Some studies have shown that the phase and morphology of particles depend on their atmospheric conditioning history, i.e., the number of drying and humidification cycles and the drying rate. 32,33 In our system, all of the SSA sampled from the headspace of the wave flume was first equilibrated to ~20% RH through a diffusion dryer and then rehumidified to a targeted RH prior to measuring the particle bounce. While there is no indication that the SSA sampled from the wave flume effloresced during this step, as noted by the liquidlike phase state of the prebloom SSA, and previously SSA was shown to not exhibit the initial stages of efflorescence until <20% RH, 34 it is important to note this difference compared with the ambient marine atmosphere, in which SSA is initially exposed to high RH near the ocean surface and then gradually dehydrates at lower RH as the SSA is lofted to higher altitudes. Figure 2 shows how the BF of SSA generally changed with RH under these conditions, segmented by stage of the bloom. The data used in the box plots

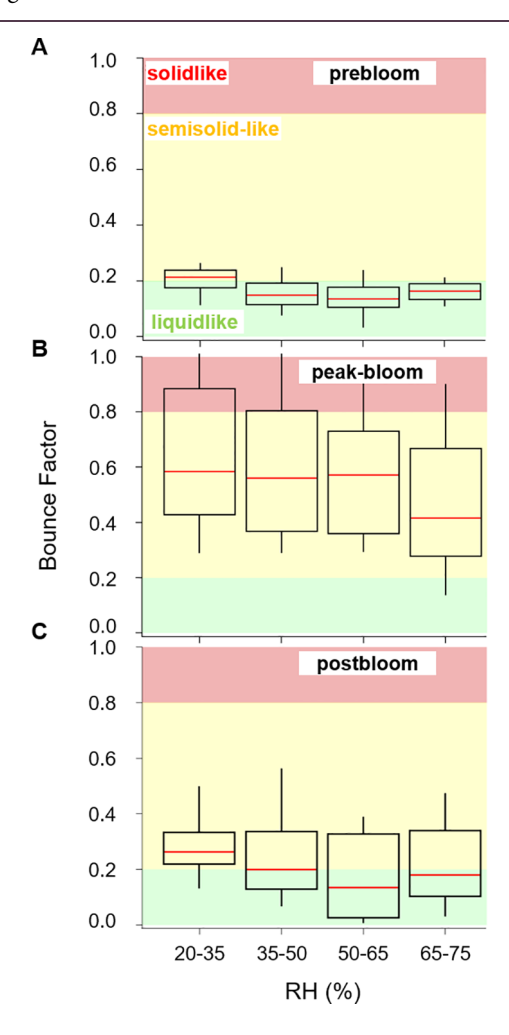


Figure 2. Box plots of bounce factor as a function of a range of relative humidity categorized by phase of the bloom, where the red line indicates the median bounce factor, the 75th percentiles are bounded by the boxes, and the 95th percentiles are represented by the whiskers. (A) Prebloom (July 28–August 2), (B) peak-bloom (August 2–5), and (C) postbloom (August 5–12). Shading indicates potential phase states of SSA based on their measured bounce factor: liquidlike (BF < 0.2), semisolid-like (0.2 \leq BF \leq 0.8), and solidlike (BF > 0.8) phase states. ^{29,35,36}

presented in Figure 2 are provided in Figure S4, separated out by day and RH cycle, and show that BF is less dependent on RH and more dependent on the stage of the phytoplankton bloom. Representative median size distributions of SSA measured by the ELPI+ and combined SEMS+APS for each RH range and stage of the bloom are provided in Figure S5. These size distributions demonstrate that when particles do not bounce or remain liquid, there is insufficient buildup of current (i.e., particles) in the bottom stages of the impactor, leading to a large discrepancy in the size distribution measured by the ELPI+ compared to that from the SEMS+APS, as observed in the prebloom stage in Figure S5A. This was due to the low number concentration of SSA in this study, which was below the theoretical minimum particle number concentration required for detection in the ELPI+ stages with 50% cutoff diameters smaller than $\sim 0.1 \ \mu m$.

The median BF during prebloom (Figure 2A) was ≤ 0.2 across all RH, which previous work suggests are mostly liquid particles, even at $20\% \le RH \le 35\%$, below the ERH of NaCl. ^{29,35,36} Further increasing RH above the DRH of NaCl did not significantly decrease the BF of these already liquid particles. If SSA were entirely sea salt (NaCl), the particles would always bounce (remain solid or crystalline) in our system up until the DRH of NaCl (~75%), at which point the particles would deliquesce and become liquid. 12,31 This was not the case during the prebloom stage. To confirm the pure sea salt aerosol bounces at low RH using our method, in a separate analysis we measured the BF of SSA produced from artificial seawater in a MART in the absence of organic matter. The results shown in Table S2 indicate that pure sea salt particles bounce with a BF of \sim 0.9 when effloresced (\sim 20% RH). In contrast, organic components that are abundant in SSA prior to phytoplankton bloom growth (monosaccharides and short-chain fatty acids)37 such as glucose and oleic acid have significantly smaller BFs of <0.1 at the same RH, as shown in Table S2. Over the 5 days of measurements during the prebloom stage, the median organic mass fractions (f_{org}) of submicron SSA measured concurrently with BF by a highresolution aerosol mass spectrometer (HR-AMS) as shown in Figure S6 varied between \sim 0.6 and \sim 0.8. These relatively large organic mass fractions suggest that the SSA phase state would be more impacted by the organic material than dissolved inorganic salts during the prebloom stage, but this depends on the molecular properties of the organic material and its hygroscopicity.

In contrast, during the peak of the bloom (Figure 2B), SSA exhibited more viscous semisolid-like phase states at low RH given the larger median BF~0.6. The median BF remained relatively stagnant but exhibited a slight decrease at RH = 65-75%, near the DRH of sea salt, though the difference is not statistically significant given the large interquartile ranges. The measured larger BF of SSA during this stage of the bloom is consistent with observations in a previous wave flume phytoplankton bloom study during IMPACTS (Investigation into Marine Particle Chemistry and Transfer Science),²² which showed from offline measurements that the organic shell of submicron SSA at 60% RH during the prebloom stage exhibited liquid/semisolid phase states but transitioned to entirely semisolid during the peak of the bloom. In that study, the more viscous phase state of SSA during the peak bloom stage was attributed to a larger volume fraction of organic material in the particles analyzed. As shown in Figure S6, however, HR-AMS measurements indicated that f_{org} was

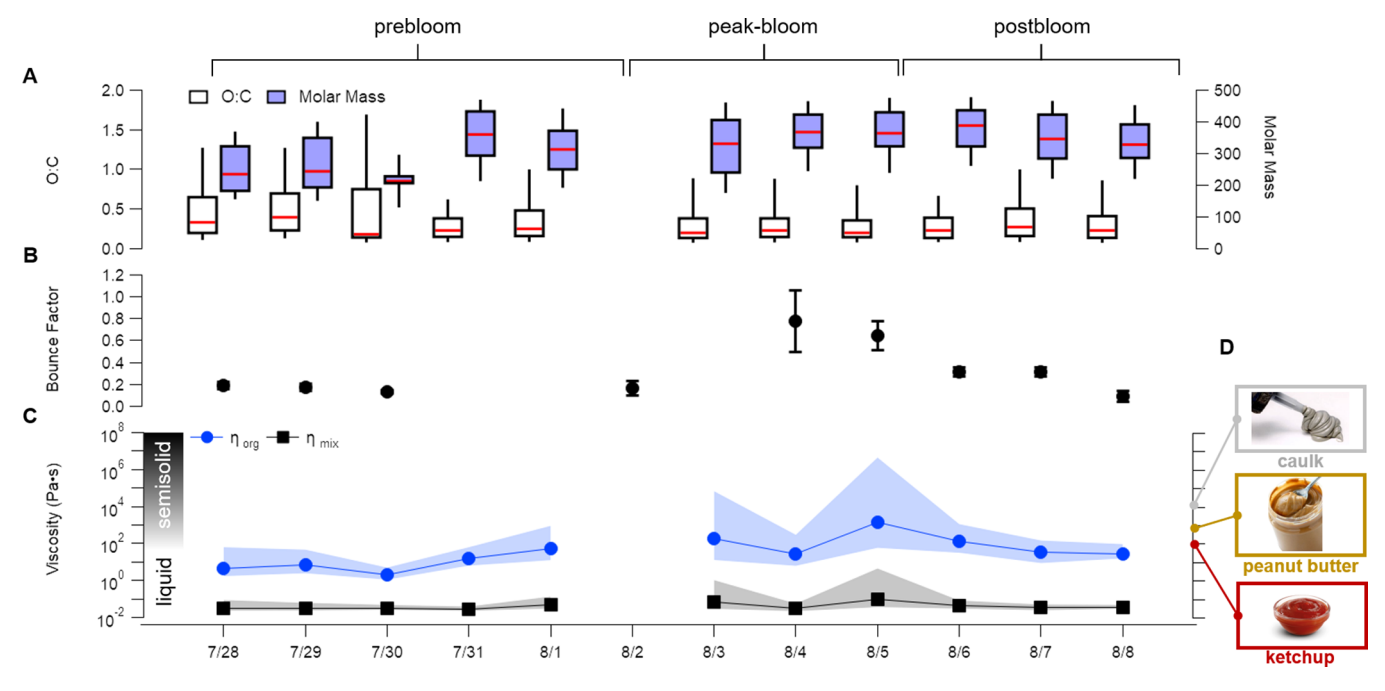


Figure 3. Daily averaged particle chemical properties and estimated η of SSA. (A) Box plots of SSA molar mass and O:C determined from EESI-TOF mass spectra. Median values are indicated by the red bar. (B) Median BF for each day of the bloom, with uncertainties shown as 1 standard deviation from the mean BF at ~50% RH. (C) Estimated η of the organic components in SSA (η_{org}) (blue) and the mixed aqueous organic and inorganic salt components in SSA (η_{mix}) (black). Shaded regions in η_{org} and η_{mix} are uncertainties propagated from the interquartile of the molar mass, O:C, and κ . The color bar indicates the approximate transition in η from semisolid to liquid, defined as 10^2 Pa·s as discussed in the text. (D) Approximate range of η of common household items for comparison. Values on August 2 are missing because of instrument maintenance on that day without compositional data.

variable during peak bloom and lower than the prebloom stage, ranging from \sim 0.3 to \sim 0.6, although the measured organic ion mass concentrations on 8/3 and 8/5 were only 2σ above the detection limit (see Figure S6).

As the bloom progressed to the postbloom stage, the measured lower BF compared to peak-bloom indicates that the SSA particles returned to a more liquidlike state, although the median BF of >0.2 in the RH range of 20–35% suggests that the particles may be semisolid-like at this low RH. While increasing RH caused the median BF of SSA to decrease from >0.2 at the lowest RH to a minimum median BF of \sim 0.1 (liquidlike) in the RH range of 50–65%, the large interquartile ranges suggest that the decrease is insignificant.

2.3. Estimated SSA Viscosity from Molecular Compo**sition.** Currently, direct measurements of the viscosity (η) of aerosol particles with diameters in the size range of SSA are not achievable and require indirect measurements, e.g., via light scattering, shape relaxation, scanning electron microscopy (SEM) imaging, and particle rebound (particle bounce),³⁸ as done here. To better understand the mechanisms and molecular drivers of the BF and phase state of SSA over the phytoplankton bloom, we analyzed bulk compositional properties of the SSA online, including particle molar mass (M) and O:C ratio of the organic compounds in SSA by extractive electrospray ionization high-resolution mass spectrometry (EESI-TOF) (see section 4.4), organic and inorganic ion mass concentrations by HR-AMS, and the hygroscopicity parameter (κ) using a CCN counter.^{39,40} We first discuss how these variables evolved during the phytoplankton bloom and then apply them to estimate the liquid-water-dependent glass transition temperature $(T_{\rm g, org, w})$ and η of the organic components in SSA $(\eta_{\rm org})$ and contrast with the η value obtained assuming that the organic components are internally and homogeneously mixed with aqueous inorganic salt (η_{mix}).

The HR-AMS-derived f_{org} values shown in Figure S6 indicate that the submicron portion of SSA was enriched with organic material during the prebloom and postbloom stages, with median f_{org} ranging from \sim 0.6 to \sim 0.8. In contrast, on August 3 and 5, corresponding to the peak bloom stage, f_{org} was \sim 0.4 and \sim 0.3, respectively. The $f_{\rm org}$ data were used to estimate the hygroscopicity parameter of the organic material in SSA (κ_{org}) on the basis of the measured κ and the volume mixing rule,³⁹ as discussed in the Supporting Information. Here, κ was measured continuously and calculated on the basis of the measured critical supersaturation of dry 60 nm SSA particles after the supersaturation was scanned from 0.05 to 0.7.⁴¹ Daily averaged κ values $(\pm 1\sigma)$ are shown in Table S3. The κ values observed across the bloom ranged from \sim 0.9 (lower bound; -1σ) to ~ 1.5 (upper bound; $+1\sigma$) with a daily averaged observed κ between \sim 1.0 and \sim 1.3 across the bloom. Similar κ values for primary SSA particles during an induced phytoplankton bloom were measured by Collins et al.41 The hygroscopicity parameter of the inorganic portion of SSA (κ_{inorg}) was applied as $\kappa_{\text{inorg}} = 1.51$ for NaCl, ⁴² which is close to the upper bound in the observed κ . Given the relatively larger organic fractions and high κ values measured during the prebloom and postbloom stages, $\kappa_{\rm org}$ was large and estimated to vary between ~0.7 and ~1.0 during these stages of the phytoplankton bloom upon application of the volume mixing rule. While the drivers of this high $\kappa_{\rm org}$ are not clearly known, another study showed that hygroscopic growth factors of SSA remain unchanged even with relatively high organic volume fractions, possibly because of surface tension suppression by surface-active organic molecules in SSA.⁴³ The presence of

highly water-soluble organic compounds could also contribute to this relatively high $\kappa_{\rm org}$. Marsh et al. 44 found that glycine, a major fraction of the amino acids in SSA, 45,46 had $\kappa_{\rm org} \sim 0.7$. In contrast, for days with low $f_{\rm org}$ (peak-bloom), $\kappa_{\rm org}$ was ~ 0.5 on August 3 and ~ 0.3 on August 5, in closer agreement with the previously measured values for organic aerosol species. 39

Measurements by EESI-TOF enabled online detection of a range of molecular ions extractable from SSA. EESI-TOF mass spectra from the prebloom and peak-bloom stages and raw background and sample ion intensities of one organic component (C₁₁H₂₁O₂⁻, possibly undecanoic acid) measured in SSA are provided in Figure S7, highlighting the sensitivity of the technique. Concentrations of unsaturated fatty acids in SSA have been measured to be on the order of 20-100 ng m⁻³, although their concentrations in this study are unknown and may change depending on how much total SSA mass was generated. However, the measured detection limit of organic compounds in SSA, based on external calibrations performed in the lab, was conservatively around tens of nanograms per cubic meter, approximately an order of magnitude less than the concentrations of several organic compounds identified in SSA in previous studies, 2 although those below the detection limit or not extractable by the EESI droplets would not have been measured. Here we report how molecular properties (M and O:C for CH and CHO compounds only) of SSA evolved daily throughout the phytoplankton bloom, as shown in Figure 3A. During SeaSCAPE, M was at a minimum during the prebloom stage, with the lowest median value of ~200 g mol⁻¹ on July 31. M of SSA was maximum (\sim 380 g mol⁻¹) between August 4 and August 6, corresponding to the peak-bloom stage and the start of the postbloom stage. O:C did not vary significantly throughout the bloom on a daily time scale, with median values between ~ 0.3 and ~ 0.4 . This range of M for SSA is comparable to that measured previously for SSA generated in a wave flume mesocosm (between ~ 160 and ~ 300 g mol⁻¹), although there are two important differences between the two studies. The previous analysis was conducted offline from aerosol filter samples using high-performance liquid chromatography tandem mass spectrometry, and the average molar mass was weighted by the ion intensity. In Figure 3A, the molar mass of SSA is reported as an unweighted median. Figure S8 shows the difference between the unweighted and weighted median molar masses of SSA. They exhibit a similar trend across the bloom, with the weighted molar mass about 15% less, on average, than the unweighted molar mass. Therefore, it is possible that the relatively larger *M* in our study compared with that reported by Cochran et al.5 results from incorporating peaks that have lower overall ion intensity in the higher mass range yet remain statistically significant above the

Materials with $\eta > 10^{12}$ Pa·s are considered to be solidlike, those with $\eta = 10^2 - 10^{12}$ Pa·s have been defined as semisolid, and those with $\eta < 10^2$ Pa·s have been defined as liquid. ¹² We first estimated $\eta_{\rm org}$ (blue curve in Figure 3C) for each day of the study at 50% RH (the same RH at which the BF data shown in Figures 1 and 3B were measured) on the basis of the trends observed in M, O:C, and $\kappa_{\rm org}$. Details of the $\eta_{\rm org}$ calculations are provided in the Supporting Information and eqs S1–S7. The viscosity of the aqueous salt solution at 50% RH was calculated separately and then combined with $\eta_{\rm org}$ to estimate the viscosity of the aqueous SSA mixture, $\eta_{\rm mix}$ (black curve in Figure 3C) for each day of the bloom. Details of the calculation of $\eta_{\rm mix}$ are provided in the Supporting Information

and eqs S8 and S9. The estimated $\eta_{\rm org}$ was lower during the prebloom stage and increased during the peak bloom stage, consistent with the increase in BF observed between these two stages of the bloom. During the prebloom stage, we estimate that $\eta_{\rm org}$ was in the range of $\sim 10^0 - 10^2$ Pa·s, similar to those of other liquid materials, including ketchup and honey. $\eta_{
m org}$ increased during the peak bloom to on average ~103 Pa·s, with propagated uncertainties in $\eta_{\rm org}$ between $\sim 10^1$ and 10^7 Pa s. Like the observed BF, $\eta_{\rm org}$ decreased into the postbloom stage following the peak of the phytoplankton bloom. Assuming that the SSA was a homogeneous internal mixture of aqueous salt and organic material, we estimate that η_{mix} would be significantly less than $\eta_{\rm org}$. During the prebloom stage, η_{mix} was ~0.005 Pa·s, and then it increased to ~10¹ Pa·s during peak bloom. Like the observed BF, both $\eta_{
m org}$ and $\eta_{
m mix}$ increased significantly during the peak bloom stage, followed by a decrease during the postbloom stage. Since it remains unclear whether the SSA particles sampled here were homogeneous internal mixtures of aqueous inorganic salt and organic carbon, with some studies indicating that SSA in the submicron range can be phase-separated core-shell-type particles^{22,47} or external mixtures of homogeneous organic carbon/inorganic salt and phase-separated particles, 47 we caution that η_{mix} is applicable only to the homogeneously mixed SSA. As a result of the development of a crystalline inorganic phase and the salting out of less water-soluble organic species with increasing salt mole fraction during phase separation, ⁴⁸ one would expect η of these particles to be closer to or greater than $\eta_{
m org}$ compared to $\eta_{
m mix}$. Thus, $\eta_{
m mix}$ may be viewed as a lower limit of the true η of SSA. The factors driving the increase in $\eta_{\rm org}$ during the peak-bloom stage are the increase in M and decrease in $\kappa_{\rm org}$, consistent with that observed for ambient aerosol particles sampled in a forested environment, which were more liquidlike with lower M and higher $\kappa_{
m org}$ and more solidlike with higher M and lower $\kappa_{
m org}$. In addition, the estimated increase in η during the peak-bloom stage is comparable to one previous offline measurement of SSA phase state during an induced phytoplankton bloom, whereby a shift in the phase state of SSA occurred from liquid and semisolid states during the prebloom phase to entirely semisolids at 60% RH during the peak of the bloom.²² Other mechanisms not taken into account here may also play a role in the observed trends in particle bounce and estimated viscosity. For example, previous work has shown that divalent cations (e.g., Ca2+ and Mg2+) can cross-link oligosaccharides, which increases molecular aggregation in SSA to create gel-like phases. 49,50 More recently, this molecular aggregation has been shown to decrease the rate of HNO₃ uptake in SSA.⁵¹ However, further work is needed to confirm how such aggregation can impact the phase state and observed BF of SSA. In addition, deriving numerical relationships between BF and η from such field data remains controversial, ^{29,38} so we do not maintain that the estimated $\eta_{
m org}$ and $\eta_{
m mix}$ here directly translate to BF. The viscosity estimation from M and O:C also does not consider heteroatom-containing organic compounds such as organic nitrates and organic sulfates but includes only CH and CHO compounds. Previous work has shown that, e.g., organic nitrate aerosol is viscous and can slow gas partitioning at the aerosol interface and diffusion of semivolatile organic compounds into the aerosol phase. 29,52,53 Organic sulfates are associated with oligomer formation and thus larger average aerosol M and T_{g} , potentially increasing the viscosity.^{29,54,}

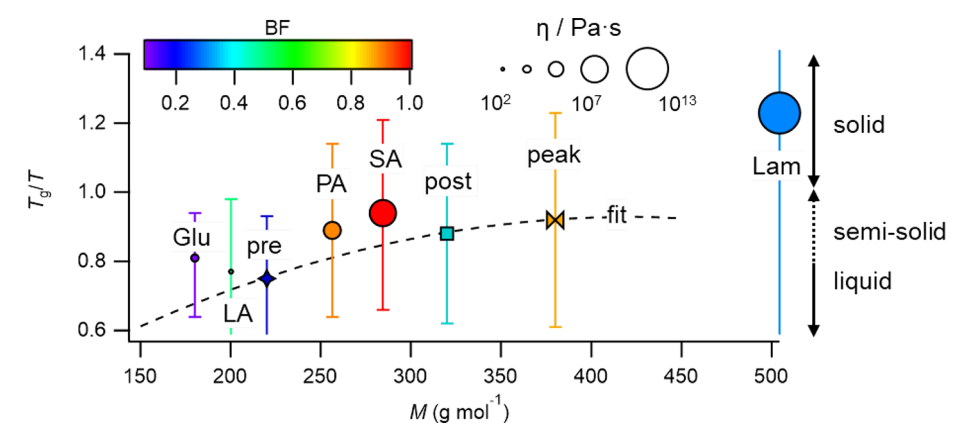


Figure 4. Calculated $T_{\rm g}/T$ as a function of the molar mass of single-component organic aerosol particles (Glu, glucose; LA, lauric acid; PA, palmitic acid; SA, stearic acid; Lam, laminarin) generated via atomization in the lab. The points are colored by their measured BF values, and the marker sizes reflect the estimated viscosities. For comparison, prebloom (pre), peak-bloom (peak), and postbloom (post) median $T_{\rm g}/T$ values are shown. The dashed line represents the fitted $T_{\rm g}/T$ incorporating a median O:C of 0.3 for the organic compounds in SSA. Error bars reflect the uncertainties in the fitting parameters used to calculate $T_{\rm g,org}$. The data used for the lab-generated aerosol are provided in Table S2.

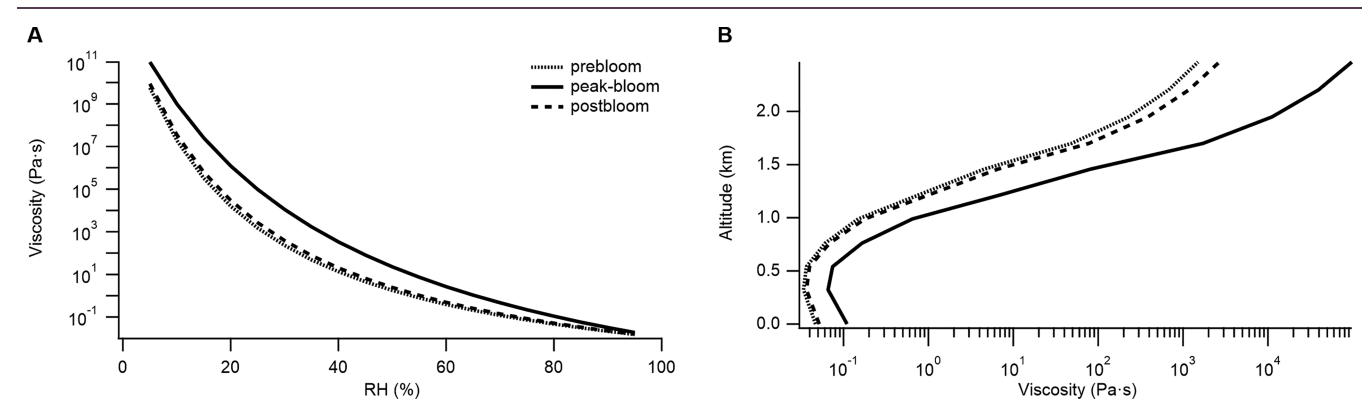


Figure 5. (A) Predicted viscosity of the organic material in SSA for each stage of the phytoplankton bloom as a function of relative humidity. (B) Estimated changes in viscosity with altitude over the ocean under cloud-free conditions. Temperature and RH profiles are provided in Figure S9.

Further work is warranted to understand their impacts on SSA viscosity.

3. CONCLUSIONS AND ATMOSPHERIC IMPLICATIONS

Our results demonstrate that the RH-dependent BF and estimated η of SSA changes during a phytoplankton bloom corresponding to changes in the biological activity of seawater, inferred from concentrations of Chl-A. An independent mesocosm study showed this to be reproducible. The phase states of SSA particles generated from seawater with low biological activity, as in the prebloom phase, are mostly liquid and marked by organic compounds with relatively low M and predicted high κ_{org} , which may be mixed free saccharides, short-chain fatty acids, and amino acids such as glycine. 37,44-46 Independent measurements of the BF of glucose, a representative monosaccharide, and oleic acid, a representative short-chain fatty acid, show these to be potential drivers of the lower M, calculated $\eta_{
m org}$, and measured BF during the prebloom stage. As the bloom progressed into the peakbloom stage, higher-molecular-weight organic compounds were detected in SSA; previous studies showed these to be polysaccharides from transparent exopolymers (TEPs) and long-chain fatty acids. 37,56,57 In Figure 4, we show the measured BF, calculated T_g/T , and estimated phase states of several representative SSA organic compounds of different

molecular sizes (a free saccharide, saturated fatty acids with different chain lengths, and a polysaccharide) in comparison with the median $T_{\rm g}/T$ during the three stages of the phytoplankton bloom.

One such polysaccharide, laminarin ($C_{18}H_{32}O_{16}$; M = 504.4g mol⁻¹), had a measured upper-bound BF of \sim 0.3, which is greater than that measured for the free saccharide glucose $(C_6H_{12}O_6; M = 180.2 \text{ g mol}^{-1})$ (BF < 0.1), illustrating the potential role of representative individual organic molecules in the phase state of SSA and increase in SSA viscosity between the prebloom and peak-bloom stages of phytoplankton growth. As illustrated in Figure 4, increasing the molecular size (chain length) of the saturated fatty acid led to higher predicted viscosities and larger BFs. Shorter-chain lauric acid (LA) $(C_{12}H_{24}O_2; M = 200.3 \text{ g mol}^{-1})$ had a BF of $\sim 0.5 (\pm 0.2)$ and a calculated T_g/T of 0.77 (+0.21/-0.20), indicating a liquid/ semisolid phase state (estimated viscosity between 10² and 10³ Pa·s under the conditions of the measurement). In contrast, longer-chain palmitic acid (PA) ($C_{16}H_{32}O_2$; M = 256.4 g mol^{-1}) and stearic acid (SA) (C₁₈H₃₆O₂; $M = 284.5 \text{ g mol}^{-1}$) aerosols produced BFs of $\sim 0.9~(\pm 0.1)$ and ≥ 1.0 and $T_{\rm g}/T$ values of 0.89 (\pm 0.25) and 0.94 (\pm 0.27/ \pm 0.28), respectively, indicating solid/semisolid phase states. The estimated viscosities for the PA and SA aerosols generated in the lab were $\sim 10^6$ and $\sim 10^8$ Pa·s, respectively, near the $\eta_{\rm org}$ upper bound of $\sim 10^7$ Pa·s during peak bloom in this study. As the phytoplankton are digested and degraded by bacteria in the postbloom phase, 58 we expect on the basis of previous observations 37 that hydrophobic intracellular material, including lipids, long-chain fatty acids and TEP are also released and degraded enzymatically. 59 Such degradation may lyse higher-molecular-weight polysaccharides and fatty acids, creating free saccharides and shorter-chain fatty acids that contribute to the decrease in M and increase in $\kappa_{\rm org}$ observed in this study during postbloom, as κ is roughly inversely proportional to $M.^{60}$

The observed changes in BF and η depending on stage of the bloom have important implications for several aerosol processes, including changes in the diffusion rates of gases and molecules in the particle phase. In Figure 5A, $\eta_{\rm org}$ is shown as a function of RH from 0% to 100%. The values were obtained by applying the Gordon-Taylor approximation (eqs S1-S5) using the median M and O:C of SSA for each stage of the phytoplankton bloom. We estimate that during the prebloom stage, characterized by low phytoplankton primary productivity, the organic material in nascent SSA particles are lowviscosity semisolids but transition to liquids at \sim 40% RH ($\eta \sim$ 10² Pa·s). Under these conditions during this stage of the bloom, SSA would have a short mixing time (nanoseconds for 100 nm particles), potentially leading to rapid diffusion of semivolatile compounds and reactive gases into the particle bulk. 28,61 On the other hand, we predict that during the peakbloom stage, SSA organic material is primarily in a viscous semisolid phase state and transitions to liquids at ~55% RH. During this stage of the bloom, the equilibrium mixing times for 100 nm particles would be on the order of seconds to several minutes and for larger, supermicrometer particles may be up to an hour or longer. Diffusion rates are crucial, as they control the potential for gaseous pollutant transport and the atmospheric lifetime of organic compounds in the aerosol phase.

The connections between biological activity in seawater and the phase state of the organic material in SSA have important implications for atmospheric composition and chemistry and the hydrological cycle. In Figure 5B, viscosity is calculated as a function of altitude on the basis of vertical profile data of temperature and RH over the marine environment for cloudfree conditions (Figure S9). Because of the high RH between the ocean surface and ~0.5 km (>80%), SSA organic material is predicted to be in a liquid state regardless of the stage of the phytoplankton bloom on the basis of our viscosity estimates. At higher altitudes, the RH decreases, and we therefore predict that SSA organic material during peak bloom can become semisolid (>10² Pa·s) above ~1.2 km in the simulation. Prebloom SSA organic material is expected to transition to semisolids at higher altitudes (~1.7 km). Greater divergence in the estimated viscosities between prebloom and peak bloom occurs at even higher altitudes. In the case of a cloud-topped marine boundary layer, supersaturated conditions would likely drive all SSA organic material to the liquid phase state near the cloud, resulting in a sharp decrease in viscosity near cloud level, unlike the estimated profile shown in Figure 5B. Furthermore, a stronger temperature inversion at the cloud top may decrease the extent of vertical mixing of SSA to the free troposphere. These results have important implications for processes such as ice nucleation. For example, viscous (glassy) aerosol particles more efficiently act as depositional icenucleating particles, potentially altering the formation and properties of cirrus clouds. 62-65 In an earlier study, addition of saccharides to simulated sea salt aerosol formed a glassy matrix,

which led to more efficient heterogeneous IN.66 Changes in the population and abundance of oceanic phytoplankton may affect the mass fraction and composition of the organic carbon emitted as SSA and thus the viscosity. 67-70 In view of the prolonged decrease in overall global concentrations of phytoplankton in oceanic environments, such as along the lower latitudes of the North and South Atlantic and Pacific oceans,⁶⁸ the potential modulations in SSA viscosity would have important global implications in terms of coastal pollutant propagation and impacts on the hydrological cycle via changes in IN efficiency. It is important to note as well that this study considers the changes in phase state of only the organic portion of nascent SSA produced from a phytoplankton bloom induced from seawater collected off the coast of southern California. Changes in nutrient availability in different locations around the world, heterogeneous reactions with SSA,² and secondary marine aerosol may potentially impact the chemical composition and phase states of aerosol in the ambient marine atmosphere different from what was observed in this study. Future studies aimed at measuring the SSA phase state in the ambient marine atmosphere would therefore be highly valuable to fully understand their impacts on atmospheric chemistry and composition and the hydrological

4. EXPERIMENTAL DESCRIPTION AND SAMPLING METHODS

4.1. SeaSCAPE Experimental Description. The NSF-CAICE SeaSCAPE study was conducted at the Scripps Institution of Oceanography Hydraulics Lab in La Jolla, CA, during the summer of 2019 (July 3-August 14). Details of the wave flume experiment, including operation of the wave flume and the resulting bubble and SSA size distributions, can be accessed from previous studies.8,27 Briefly, seawater was collected from Scripps Pier (La Jolla, CA; 32° 51′ 56.8″ N; 117° 15' 38.48" W) and filtered (50 μ m Nitex mesh) to remove grazing zooplankton before the introduction of f/2 growth nutrients to the wave flume. 10,22,37 Fluorescent lights were attached to the walls of the wave flume and operated on timers to simulate diurnal light cycles for phytoplankton growth (lights on 7 AM-9 PM), although the SSA phase state measurements were carried out overnight in the absence of light. The growth and activity of the phytoplankton population were approximated by the concentration of Chl-A in the wave flume, a common measure of algal biomass,⁷¹ and used in this study to associate the measured BF with biological activity in

4.2. Nascent Sea Spray Sampling Apparatus. Nascent SSA was sampled at a flow rate of 5 liters per minute (lpm), first through a home-built Carulite denuder (Ozone Solutions) to scrub ozone (15 \pm 5 ppb on average in the wave flume headspace as measured using a 2B Technologies O₃ monitor) and volatile organic compounds (VOCs) (2 ± 1 ppb as measured by a Tofwerk Vocus proton transfer reaction mass spectrometer (PTR-TOF)) and then through a home-built silica diffusion dryer to equilibrate the RH to ~20%. All of the tubing was stainless steel to maximize particle transmission through the sampling lines and minimize offgassing of adsorbed semivolatile species. On the basis of particle transmission efficiency measurements, aerosol particle losses in our apparatus were insignificant (<5%) after correction for dilution. The sample was diluted with different ratios of dry and water-saturated zero air mixtures at a fixed flow rate of ~7

lpm to vary RH. Saturated air was generated by bubbling zero air from a zero-air generator (AADCO) through ultrahighpurity Milli-Q water (deionized; resistivity = 18.2 M Ω /cm) by calibrated mass flow controllers (Alicat Scientific). The RH and temperature of the sample flow were continuously monitored with an RH/temperature sensor (Sensirion AG) placed in line with the sample tubing, and the RH was controlled between ~20% and ~80%. The sample flow was split four ways with a flow splitter (Brechtel, Inc., $^1/_4$ " i.d.) to the SEMS sampling at 0.3 lpm, the EESI-TOF at 1.7 lpm, the APS at 0.5 lpm, and the ELPI+ at 10 lpm as depicted in the experimental apparatus shown in Figure S1.

4.3. Online SSA Phase State Analysis. Our analysis of particle phase state is complementary to the methods outlined in an earlier study based on measurements of particle bounce, 72 with important updates discussed here. Aerosol size distributions were measured with an electrical lowpressure impactor (Dekati Ltd.), which electrically detects aerosol and separates aerosol particles on the basis of their aerodynamic diameters between 6 nm and 10 μ m at 1 Hz. Aerosols at the ELPI+ inlet are first unipolarly charged with a corona charger followed by impaction onto smooth, cleaned (wiped with methanol and Milli-Q water using a Kimwipe) aluminum-foil plates on each impactor stage to promote particle bounce as done previously. A scanning electrical mobility sizer (Brecthel Inc.) measured submicron SSA size distributions between 5 and 850 nm at a resolution of 100 bins with a total scan time of 2 min, and an aerodynamic particle sizer (TSI Inc.) measured supermicrometer SSA size distributions between 0.5 and 20 μ m in 54 bins with a scan time of 1 min. We then compared the current detected in each stage of the ELPI+ with the equivalent theoretical currents calculated from the size distributions measured by the SEMS and APS binned by the same size ranges of the ELPI+, after the SEMS and APS size distribution data were passed through the ELPI+ kernel function to account for charging efficiency and particle losses as a function of size through each impactor stage. 74,75 Particles that bounce produce a size distribution that is biased toward smaller-diameter particles in the ELPI+, as demonstrated in Figure S1 for lab-generated ammonium sulfate particles. The reduction in pressure in the ELPI+ from atmospheric pressure at the inlet to 40 mbar at the filter stage is expected to significantly decrease the RH in the impactor, which may cause the particles to dry during sampling and promote bouncing in the ELPI+. However, whether the lower RH in the impactor influences the phase state of the aerosol and observed BF depends on the particle size, the time scales for equilibration of water in the particles with the RH at each stage of the impactor, and the particle residence time at each stage. Koop et al.¹² reported that the condensed-phase diffusion coefficient of water, $D_{H,O}$, is typically between 10^{-10} and 10^{-12} cm² s⁻¹ at room temperature. Assuming a mean number-weighted particle diameter of ~200 nm during these measurements and a $D_{\rm H_2O}$ value of ${\sim}10^{-12}~{\rm cm}^2~{\rm s}^{-1}$ yields an efolding time of \sim 10 s for equilibration of water in the particles, which is 2 orders of magnitude longer than the approximate residence time of \sim 100 ms in the ELPI+. On the other hand, the e-folding time could be as short as 100 ms, assuming $D_{\mathrm{H},\mathrm{O}}$ $\sim 10^{-10}~\text{cm}^2~\text{s}^{-1}$ with shorter times for smaller particles, but significantly longer than the residence time in each stage of the impactor (\sim 5–10 ms). Thus, particles likely are in their native state during impaction in the ELPI+, as has been addressed

previously by Slade et al.,²⁹ who showed that the BF and phase state of ambient secondary organic aerosol (SOA) particles sampled in a forest environment are comparable to the phase state measurements performed offline using atomic force microscopy (AFM) at atmospheric pressure and the same RH as sampled at the inlet of the ELPI+.

To evaluate changes in the particle phase state of SSA, we calculated particle bounce factors via the difference in current measured in the ELPI+ $(I_{\mathrm{ELPI}(n)})$ from that determined from the SEMS and APS at the equivalent ELPI+ stage (n) and normalized to the total ideal current determined by the SEMS and APS $(I_{\mathrm{Ideal}(n)})$, as shown in eq 1:

$$BF = \sum_{n=1}^{12} \frac{I_{\text{ELPI} > \text{Ideal} \cdot 1.5}^{\text{ELPI} > \text{Ideal} \cdot 1.5} - I_{\text{Ideal} (n)}^{\text{ELPI} > \text{Ideal} \cdot 1.5}}{I_{\text{Ideal} (n)}^{\text{ELPI} \leq \text{Ideal} \cdot 1.5}}$$
(1)

The current associated with bounced particles in the ELPI+ was taken as that which was more than 150% of the equivalent current observed by the SEMS or APS in the same size bin. This threshold was chosen to ensure greater than 3 standard deviations difference between the measured ELPI+ current and the calculated ideal currents accounting for the uncertainties in the kernel function. The uncertainties applied here were derived from that for dioctyl sebacate aerosol particles reported by Jarvinen et al., 75 which includes a 5% uncertainty for the cut points, 10.8% for the charging efficiency, 1% for the electric current, 3% for the particle concentration, and 1% for the flow measurement. This results in a root-sum-of-squares uncertainty of 12% for particles larger than 40 nm (20% for the smallest particles). However, the uncertainty is likely greater in our measurement because of differences in charge transfer, chemical composition, and shape of the particles compared with those reported by Jarvinen et al. 75 We further analyzed the size distributions of atomized polystyrene latex (PSL) aerosol (mean diameter of 100 nm) measured by our ELPI+ (using coated sintered plates to reduce particle bounce) and our SEMS as a reference instrument. While the calculated geometric mean diameters and size distributions measured by the two instruments agreed, the ELPI+ measured an approximately 30% lower total number concentration relative to the SEMS. This has been observed in similar instrument intercomparisons with the ELPI using PSL and ${\rm TiO_2}$ aerosol. 76,77 Considering these differences, we estimate that the overall uncertainty may be as large as 50%.

In this study, excess current was observed in both the bottom stages of the impactor (from bouncing of submicron SSA) and the upper stages of the impactor (from bouncing of supermicrometer SSA), which was not observed in previous studies that focused primarily on bounce measurements of submicrometer SOA particles. 29,73,78-80 Thus, the BF from eq 1 is defined explicitly as the fraction of the total aerosol current associated with the aerosol that bounces upon impaction in the ELPI+ and includes both sub- and supermicrometer SSA. It is important to note, however, that because of the low total SSA number concentration in this study, it is possible that the number concentration in the bottom stages of the ELPI+ was below the nominal minimum number of particles needed for detection. This would lead to artificially lower number concentrations measured by the ELPI+ in the bottom impactor stages compared with that measured by the SEMS, as was the case for the prebloom period shown in Figure S5A. This approach of measuring particle bounce in an impactor has been used previously to evaluate aerosol phase states from field

measurements in terrestrial environments^{29,35} and laboratory studies^{72,73,79,81} and corroborated by offline particle phase and morphology measurements employing AFM.²⁹ As discussed in the Supporting Information and shown in Table S1, we demonstrate very good agreement between the BF measured by this method and other studies employing test liquid oleic acid particles and solidlike ammonium sulfate. Table S2 further demonstrates that solid (crystalline) sea salt particles generated in the MART exhibit a BF of ~0.9, whereas low-viscosity semisolid/liquid glucose aerosol generated from a commercial atomizer and measured at 50% RH exhibits a BF of ~0.1. As suggested from earlier studies of organic-dominated aerosol, a BF of >0.8 indicates the presence of mostly solidlike particles, intermediate BF values (0.2 \leq BF \leq 0.8) indicate the presence of mostly semisolids, and low BF values (BF < 0.2) represent mostly liquidlike particles. ^{29,38,82} However, since sub- and supermicrometer SSA can both be internally and externally mixed with organic matter, sea salt, and biological material, 8,37 it is possible that different phase states exist within each size mode. Our BF measurement is dependent on the current measurement, which is driven by the particle number concentration and charge on the particle. We applied charge corrections to all particles and note that the dominant numberweighted particle size of SSA and driver of the changes in BF in this study are particles with an aerodynamic diameter of ~0.2 μ m, though some supermicrometer particles contributed to the measured BF. While further work is warranted to isolate the BF of size-resolved SSA, it is not yet possible using our method without use of a monodisperse aerosol generator.

Measurements of BF took place overnight (in the absence of artificial light) for approximately 8 h on each day of the study. Sample RH was adjusted hourly across a range of RH as described in section 4.2. This RH cycle was repeated to provide two or three replicates at each RH value per day. One 20 min cycle (5 min at each RH set point) of BF measurements was conducted while the SSA sample was passed first through two HEPA filters as a "blank" measurement to account for any excess current measured by the ELPI+ in the absence of particles (e.g., residual ions in air).83 This current was subtracted from the sample current prior to calculation of the BF. The first and last 15 min of collected data were discarded for each RH set point to allow for equilibration inside the sampling manifold. All stages were checked for statistical outliers that strayed beyond 3 standard deviations from the mean of the following 10 min before the BF was calculated.

4.4. Extractive Electrospray Ionization High-Resolution Time-of-Flight Mass Spectrometry (EESI-TOF). EESI-TOF was used for real-time and online aerosol composition analysis. 51,84,85 Sampling was done overnight over the same sampling period as for the BF measurements with 1 s averaging (i.e., 1 s time resolution), with blanks taken before and after the nighttime sampling time. Nascent SSA was sampled at a flow rate of 1.7 lpm and was passed through a graphite-extruded denuder to remove gas-phase species and reduce background. The HrTOF-MS resolution, $m/\Delta m$, was ~ 3000 at m/z 64 (CH₃CNNa⁺) in positive mode and 59 (CH₃COO⁻) in negative mode. Both negative and positive modes were used in the experiment to expand the range of compounds detected by the instrument. Generally, while both modes are sensitive to most organic molecules in SOA, negative mode tends to be more sensitive to acidic moieties and has been employed in the analysis of metabolites in

aerosols emitted from humans and plants. 84-87 This study represents the first time EESI-TOF has been applied in the analysis of SSA composition. In positive mode, the electrospray was a 50/50 acetonitrile (>99%, Sigma-Aldrich)/water (Milli-Q) solution doped with 100 ppm NaI (>99%, Sigma-Aldrich) to produce Na⁺ and CH₃CNNa⁺ clusters. In negative mode, the electrospray was a 50/50 acetonitrile (>99%, Sigma-Aldrich)/water (Milli-Q) solution doped with 100 ppm KCH₃COOH (>99%, Sigma-Aldrich), which led to deprotonation of the sample molecules and clusters with acetate ions. The electrospray solution was pressurized to 350 mbar and charged at +2500/-2500 kV. This solution was passed through a fused-silica column with an i.d. of 50 μ m (IDEX) to create the electrospray at an angle to intercept sampled aerosol. The coalesced droplets then went through a capillary heated to 250 °C. The signal intensity reported is normalized to the charged acetonitrile signal using eq 2 in order to better compare positive and negative modes:

$$signal = \frac{I_{sample} - I_{background}}{I_{acetonitrile}}$$
(2)

The spectra were averaged every 10 s. Peaks were identified using high-resolution peak fitting and then by iterative peak analysis using Tofware 3.2.0 (Tofwerk AG, Thun, Switzerland). About 350 peaks were identified each day as statistically significantly above the measured intensity of the background ($I_{\rm background}$), defined here as the mass-to-charge ratios (m/z) with signals greater than $3\sigma_{\rm background}$ after background subtraction. We report the median molar mass and O:C for each day of the study based on the molecular formulas according to their exact masses measured by the EESI-TOF.

4.5. High-Resolution Time-of-Flight Aerosol Mass Spectrometry (HR-AMS). The chemical composition of submicrometer nonrefractory aerosol, including bulk chemical speciation and organic mass fractions, was determined by high-resolution time-of-flight aerosol mass spectrometry (HrTOF-AMS; Aerodyne, Inc.). ^{89,90} The HrTOF-AMS was operated in V-mode with standard MS mode (5 s open, 5 s closed) and PTOF (10 s) with 5 min sampling averages. The 1 min detection limit for organic aerosol was 0.082 μ g m⁻³, as determined from filter periods throughout the experiment.

ASSOCIATED CONTENT

Supporting Information

The Supporting Information is available free of charge at https://pubs.acs.org/doi/10.1021/acsearthspace-chem.1c00186.

Method comparison using standard ammonium sulfate and oleic acid aerosol, glass transition temperature and viscosity calculations for the organic components in SSA, viscosity calculation for aqueous inorganic salt and mixed SSA, Figures S1–S9, and Tables S1–S3 (PDF)

AUTHOR INFORMATION

Corresponding Author

I

Jonathan H. Slade — Department of Chemistry and Biochemistry, University of California, San Diego, La Jolla, California 92093, United States; orcid.org/0000-0002-5026-4229; Email: jhslade@ucsd.edu

Authors

- Paul R. Tumminello Department of Chemistry and Biochemistry, University of California, San Diego, La Jolla, California 92093, United States
- Reece C. James Department of Chemistry and Biochemistry, University of California, San Diego, La Jolla, California 92093, United States
- Samantha Kruse Department of Chemistry and Biochemistry, University of California, San Diego, La Jolla, California 92093, United States
- Allison Kawasaki Department of Chemistry and Biochemistry, University of California, San Diego, La Jolla, California 92093, United States
- Adam Cooper Department of Chemistry and Biochemistry, University of California, San Diego, La Jolla, California 92093, United States
- Isis Guadalupe-Diaz Department of Chemistry, University of Puerto Rico, San Juan, Puerto Rico 00931
- Karen Lopo Zepeda Department of Chemistry and Biochemistry, University of California, San Diego, La Jolla, California 92093, United States
- Daniel R. Crocker Department of Chemistry and Biochemistry, University of California, San Diego, La Jolla, California 92093, United States
- Kathryn J. Mayer Department of Chemistry and Biochemistry, University of California, San Diego, La Jolla, California 92093, United States; orcid.org/0000-0003-1179-9244
- Jonathan S. Sauer Department of Chemistry and Biochemistry, University of California, San Diego, La Jolla, California 92093, United States
- Christopher Lee Scripps Institution of Oceanography, University of California, San Diego, La Jolla, California 92093, United States
- Kimberly A. Prather Department of Chemistry and Biochemistry, University of California, San Diego, La Jolla, California 92093, United States; Scripps Institution of Oceanography, University of California, San Diego, La Jolla, California 92093, United States

Complete contact information is available at: https://pubs.acs.org/10.1021/acsearthspacechem.1c00186

Notes

The authors declare no competing financial interest.

ACKNOWLEDGMENTS

This work was funded by the NSF through NSF-CAICE under Grant CHE-1801971. The authors thank the entire SeaSCAPE team for their efforts in making the wave flume study possible. J.H.S. and P.R.T. thank Chris Cappa and Timothy Bertram for helpful discussions of the content in this article, Delphine Farmer and Lauren Garofalo for providing the HR-AMS data, Clare Morris and Francesca Malfatti for bacterial cell counts and extracted Chl-A concentrations, and Skip Pomeroy and Marissa Tessman for helpful discussions and provision of material for the MART studies.

REFERENCES

(1) Gong, S. L.; Barrie, L. A.; Lazare, M. Canadian Aerosol Module (CAM): A size-segregated simulation of atmospheric aerosol processes for climate and air quality models 2. Global sea-salt aerosol and its budgets. *J. Geophys. Res.* **2002**, *107* (D24), 4779.

- (2) Bertram, T. H.; Cochran, R. E.; Grassian, V. H.; Stone, E. A. Sea spray aerosol chemical composition: elemental and molecular mimics for laboratory studies of heterogeneous and multiphase reactions. *Chem. Soc. Rev.* **2018**, *47* (7), 2374–2400.
- (3) King, S. M.; Butcher, A. C.; Rosenoern, T.; Coz, E.; Lieke, K. I.; de Leeuw, G.; Nilsson, E. D.; Bilde, M. Investigating primary marine aerosol properties: CCN activity of sea salt and mixed inorganic-organic particles. *Environ. Sci. Technol.* **2012**, *46* (19), 10405–12.
- (4) Knopf, D. A.; Alpert, P. A.; Wang, B. The Role of Organic Aerosol in Atmospheric Ice Nucleation: A Review. ACS Earth Space Chem. 2018, 2 (3), 168–202.
- (5) Cochran, R. E.; Jayarathne, T.; Stone, E. A.; Grassian, V. H. Selectivity Across the Interface: A Test of Surface Activity in the Composition of Organic-Enriched Aerosols from Bubble Bursting. *J. Phys. Chem. Lett.* **2016**, 7 (9), 1692–6.
- (6) Lhuissier, H.; Villermaux, E. Bursting bubble aerosols. *J. Fluid Mech.* **2012**, *696*, 5–44.
- (7) Crocker, D. R.; Hernandez, R. E.; Huang, H. D.; Pendergraft, M. A.; Cao, R.; Dai, J.; Morris, C. K.; Deane, G. B.; Prather, K. A.; Thiemens, M. H. Biological Influence on $\delta 13C$ and Organic Composition of Nascent Sea Spray Aerosol. *ACS Earth Space Chem.* **2020**, 4 (9), 1686–1699.
- (8) Prather, K. A.; Bertram, T. H.; Grassian, V. H.; Deane, G. B.; Stokes, M. D.; Demott, P. J.; Aluwihare, L. I.; Palenik, B. P.; Azam, F.; Seinfeld, J. H.; Moffet, R. C.; Molina, M. J.; Cappa, C. D.; Geiger, F. M.; Roberts, G. C.; Russell, L. M.; Ault, A. P.; Baltrusaitis, J.; Collins, D. B.; Corrigan, C. E.; Cuadra-Rodriguez, L. A.; Ebben, C. J.; Forestieri, S. D.; Guasco, T. L.; Hersey, S. P.; Kim, M. J.; Lambert, W. F.; Modini, R. L.; Mui, W.; Pedler, B. E.; Ruppel, M. J.; Ryder, O. S.; Schoepp, N. G.; Sullivan, R. C.; Zhao, D. Bringing the ocean into the laboratory to probe the chemical complexity of sea spray aerosol. *Proc. Natl. Acad. Sci. U. S. A.* 2013, 110 (19), 7550—5.
- (9) Estillore, A. D.; Morris, H. S.; Or, V. W.; Lee, H. D.; Alves, M. R.; Marciano, M. A.; Laskina, O.; Qin, Z.; Tivanski, A. V.; Grassian, V. H. Linking hygroscopicity and the surface microstructure of model inorganic salts, simple and complex carbohydrates, and authentic sea spray aerosol particles. *Phys. Chem. Chem. Phys.* **2017**, *19* (31), 21101–21111.
- (10) Wang, X.; Sultana, C. M.; Trueblood, J.; Hill, T. C.; Malfatti, F.; Lee, C.; Laskina, O.; Moore, K. A.; Beall, C. M.; McCluskey, C. S.; Cornwell, G. C.; Zhou, Y.; Cox, J. L.; Pendergraft, M. A.; Santander, M. V.; Bertram, T. H.; Cappa, C. D.; Azam, F.; DeMott, P. J.; Grassian, V. H.; Prather, K. A. Microbial Control of Sea Spray Aerosol Composition: A Tale of Two Blooms. *ACS Cent. Sci.* **2015**, *1* (3), 124–31.
- (11) Dette, H. P.; Koop, T. Glass formation processes in mixed inorganic/organic aerosol particles. *J. Phys. Chem. A* **2015**, *119* (19), 4552–61.
- (12) Koop, T.; Bookhold, J.; Shiraiwa, M.; Poschl, U. Glass transition and phase state of organic compounds: dependency on molecular properties and implications for secondary organic aerosols in the atmosphere. *Phys. Chem. Chem. Phys.* **2011**, *13* (43), 19238–55.
- (13) Zobrist, B.; Soonsin, V.; Luo, B. P.; Krieger, U. K.; Marcolli, C.; Peter, T.; Koop, T. Ultra-slow water diffusion in aqueous sucrose glasses. *Phys. Chem. Chem. Phys.* **2011**, *13* (8), 3514–26.
- (14) Slade, J. H.; Shiraiwa, M.; Arangio, A.; Su, H.; Pöschl, U.; Wang, J.; Knopf, D. A. Cloud droplet activation through oxidation of organic aerosol influenced by temperature and particle phase state. *Geophys. Res. Lett.* **2017**, *44* (3), 1583–1591.
- (15) Marshall, F. H.; Miles, R. E. H.; Song, Y. C.; Ohm, P. B.; Power, R. M.; Reid, J. P.; Dutcher, C. S. Diffusion and reactivity in ultraviscous aerosol and the correlation with particle viscosity. *Chem. Sci.* **2016**, *7* (2), 1298–1308.
- (16) Slade, J. H.; Knopf, D. A. Multiphase OH oxidation kinetics of organic aerosol: The role of particle phase state and relative humidity. *Geophys. Res. Lett.* **2014**, *41* (14), 5297–5306.
- (17) Zelenyuk, A.; Imre, D. G.; Wilson, J.; Bell, D. M.; Suski, K. J.; Shrivastava, M.; Beranek, J.; Alexander, M. L.; Kramer, A. L.; Massey Simonich, S. L. The effect of gas-phase polycyclic aromatic

- hydrocarbons on the formation and properties of biogenic secondary organic aerosol particles. *Faraday Discuss.* **2017**, 200, 143–164.
- (18) Wang, X.; Deane, G. B.; Moore, K. A.; Ryder, O. S.; Stokes, M. D.; Beall, C. M.; Collins, D. B.; Santander, M. V.; Burrows, S. M.; Sultana, C. M.; Prather, K. A. The role of jet and film drops in controlling the mixing state of submicron sea spray aerosol particles. *Proc. Natl. Acad. Sci. U. S. A.* **2017**, *114* (27), 6978–6983.
- (19) Shiraiwa, M.; Li, Y.; Tsimpidi, A. P.; Karydis, V. A.; Berkemeier, T.; Pandis, S. N.; Lelieveld, J.; Koop, T.; Poschl, U. Global distribution of particle phase state in atmospheric secondary organic aerosols. *Nat. Commun.* **2017**, *8*, 15002.
- (20) Nandy, L.; Liu, S.; Gunsbury, C.; Wang, X.; Pendergraft, M. A.; Prather, K. A.; Dutcher, C. S. Multistep Phase Transitions in Sea Surface Microlayer Droplets and Aerosol Mimics using Microfluidic Wells. ACS Earth Space Chem. 2019, 3 (7), 1260–1267.
- (21) Lee, H. D.; Kaluarachchi, C. P.; Hasenecz, E. S.; Zhu, J. Z.; Popa, E.; Stone, E. A.; Tivanski, A. V. Effect of dry or wet substrate deposition on the organic volume fraction of core—shell aerosol particles. *Atmos. Meas. Tech.* **2019**, *12* (3), 2033–2042.
- (22) Lee, H. D.; Morris, H. S.; Laskina, O.; Sultana, C. M.; Lee, C.; Jayarathne, T.; Cox, J. L.; Wang, X.; Hasenecz, E. S.; DeMott, P. J.; Bertram, T. H.; Cappa, C. D.; Stone, E. A.; Prather, K. A.; Grassian, V. H.; Tivanski, A. V. Organic Enrichment, Physical Phase State, and Surface Tension Depression of Nascent Core—Shell Sea Spray Aerosols during Two Phytoplankton Blooms. ACS Earth Space Chem. 2020, 4 (4), 650–660.
- (23) Mayer, K. J.; Sauer, J. S.; Dinasquet, J.; Prather, K. A. CAICE Studies: Insights from a Decade of Ocean-Atmosphere Experiments in the Laboratory. *Acc. Chem. Res.* **2020**, *53* (11), 2510–2520.
- (24) Alderkamp, A.-C.; Buma, A. G. J.; van Rijssel, M. The carbohydrates of Phaeocystis and their degradation in the microbial food web. *Biogeochemistry* **2007**, *83* (1–3), 99–118.
- (25) Bateman, A. P.; Bertram, A. K.; Martin, S. T. Hygroscopic influence on the semisolid-to-liquid transition of secondary organic materials. *I. Phys. Chem. A* **2015**, *119* (19), 4386–95.
- (26) Lee, C.; Sultana, C. M.; Collins, D. B.; Santander, M. V.; Axson, J. L.; Malfatti, F.; Cornwell, G. C.; Grandquist, J. R.; Deane, G. B.; Stokes, M. D.; Azam, F.; Grassian, V. H.; Prather, K. A. Advancing Model Systems for Fundamental Laboratory Studies of Sea Spray Aerosol Using the Microbial Loop. *J. Phys. Chem. A* **2015**, *119* (33), 8860–70.
- (27) Stokes, M. D.; Deane, G. B.; Prather, K.; Bertram, T. H.; Ruppel, M. J.; Ryder, O. S.; Brady, J. M.; Zhao, D. A Marine Aerosol Reference Tank system as a breaking wave analogue for the production of foam and sea-spray aerosols. *Atmos. Meas. Tech.* **2013**, *6* (4), 1085–1094.
- (28) Shiraiwa, M.; Ammann, M.; Koop, T.; Poschl, U. Gas uptake and chemical aging of semisolid organic aerosol particles. *Proc. Natl. Acad. Sci. U. S. A.* **2011**, *108* (27), 11003–8.
- (29) Slade, J. H.; Ault, A. P.; Bui, A. T.; Ditto, J. C.; Lei, Z.; Bondy, A. L.; Olson, N. E.; Cook, R. D.; Desrochers, S. J.; Harvey, R. M.; Erickson, M. H.; Wallace, H. W.; Alvarez, S. L.; Flynn, J. H.; Boor, B. E.; Petrucci, G. A.; Gentner, D. R.; Griffin, R. J.; Shepson, P. B. Bouncier Particles at Night: Biogenic Secondary Organic Aerosol Chemistry and Sulfate Drive Diel Variations in the Aerosol Phase in a Mixed Forest. *Environ. Sci. Technol.* 2019, 53 (9), 4977–4987.
- (30) Song, M.; Marcolli, C.; Krieger, U. K.; Lienhard, D. M.; Peter, T. Morphologies of mixed organic/inorganic/aqueous aerosol droplets. *Faraday Discuss.* **2013**, *165*, 289–316.
- (31) Gupta, D.; Eom, H. J.; Cho, H. R.; Ro, C. U. Hygroscopic behavior of NaCl-MgCl2 mixture particles as nascent sea-spray aerosol surrogates and observation of efflorescence during humid-ification. *Atmos. Chem. Phys.* **2015**, *15* (19), 11273–11290.
- (32) Lu, J. W.; Rickards, A. M.; Walker, J. S.; Knox, K. J.; Miles, R. E.; Reid, J. P.; Signorell, R. Timescales of water transport in viscous aerosol: measurements on sub-micron particles and dependence on conditioning history. *Phys. Chem. Chem. Phys.* **2014**, *16* (21), 9819–30.

- (33) Altaf, M. B.; Freedman, M. A. Effect of Drying Rate on Aerosol Particle Morphology. J. Phys. Chem. Lett. 2017, 8 (15), 3613–3618.
- (34) Patterson, J. P.; Collins, D. B.; Michaud, J. M.; Axson, J. L.; Sultana, C. M.; Moser, T.; Dommer, A. C.; Conner, J.; Grassian, V. H.; Stokes, M. D.; Deane, G. B.; Evans, J. E.; Burkart, M. D.; Prather, K. A.; Gianneschi, N. C. Sea Spray Aerosol Structure and Composition Using Cryogenic Transmission Electron Microscopy. ACS Cent. Sci. 2016, 2 (1), 40–47.
- (35) Pajunoja, A.; Hu, W.; Leong, Y. J.; Taylor, N. F.; Miettinen, P.; Palm, B. B.; Mikkonen, S.; Collins, D. R.; Jimenez, J. L.; Virtanen, A. Phase state of ambient aerosol linked with water uptake and chemical aging in the southeastern US. *Atmos. Chem. Phys.* **2016**, *16* (17), 11163–11176.
- (36) Pajunoja, A.; Lambe, A. T.; Hakala, J.; Rastak, N.; Cummings, M. J.; Brogan, J. F.; Hao, L.; Paramonov, M.; Hong, J.; Prisle, N. L.; Malila, J.; Romakkaniemi, S.; Lehtinen, K. E. J.; Laaksonen, A.; Kulmala, M.; Massoli, P.; Onasch, T. B.; Donahue, N. M.; Riipinen, I.; Davidovits, P.; Worsnop, D. R.; Petäjä, T.; Virtanen, A. Adsorptive uptake of water by semisolid secondary organic aerosols. *Geophys. Res. Lett.* 2015, 42 (8), 3063–3068.
- (37) Cochran, R. E.; Laskina, O.; Trueblood, J. V.; Estillore, A. D.; Morris, H. S.; Jayarathne, T.; Sultana, C. M.; Lee, C.; Lin, P.; Laskin, J.; Laskin, A.; Dowling, J. A.; Qin, Z.; Cappa, C. D.; Bertram, T. H.; Tivanski, A. V.; Stone, E. A.; Prather, K. A.; Grassian, V. H. Molecular Diversity of Sea Spray Aerosol Particles: Impact of Ocean Biology on Particle Composition and Hygroscopicity. *Chem* **2017**, *2* (5), 655–667.
- (38) Reid, J. P.; Bertram, A. K.; Topping, D. O.; Laskin, A.; Martin, S. T.; Petters, M. D.; Pope, F. D.; Rovelli, G. The viscosity of atmospherically relevant organic particles. *Nat. Commun.* **2018**, 9 (1), 956.
- (39) Petters, M.; Kreidenweis, S. M. A single parameter representation of hygroscopic growth and cloud condensation nucleus activity. *Atmos. Chem. Phys.* **2007**, *7* (8), 1961–1971.
- (40) Petters, M.; Kreidenweis, S. M. A single parameter representation of hygroscopic growth and cloud condensation nucleus activity Part 2: Including solubility. *Atmos. Chem. Phys.* **2008**, 8 (20), 6273–6279.
- (41) Collins, D. B.; Zhao, D. F.; Ruppel, M. J.; Laskina, O.; Grandquist, J. R.; Modini, R. L.; Stokes, M. D.; Russell, L. M.; Bertram, T. H.; Grassian, V. H.; Deane, G. B.; Prather, K. A. Direct aerosol chemical composition measurements to evaluate the physicochemical differences between controlled sea spray aerosol generation schemes. *Atmos. Meas. Tech.* **2014**, *7* (11), 3667–3683.
- (42) Topping, D.; Barley, M.; Bane, M. K.; Higham, N.; Aumont, B.; Dingle, N.; McFiggans, G. UManSysProp v1.0: an online and open-source facility for molecular property prediction and atmospheric aerosol calculations. *Geosci. Model Dev.* **2016**, *9* (2), 899–914.
- (43) Cravigan, L. T.; Mallet, M. D.; Vaattovaara, P.; Harvey, M. J.; Law, C. S.; Modini, R. L.; Russell, L. M.; Stelcer, E.; Cohen, D. D.; Olsen, G.; Safi, K.; Burrell, T. J.; Ristovski, Z. Sea spray aerosol organic enrichment, water uptake and surface tension effects. *Atmos. Chem. Phys.* **2020**, 20 (13), 7955–7977.
- (44) Marsh, A.; Miles, R. E. H.; Rovelli, G.; Cowling, A. G.; Nandy, L.; Dutcher, C. S.; Reid, J. P. Influence of organic compound functionality on aerosol hygroscopicity: dicarboxylic acids, alkylsubstituents, sugars and amino acids. *Atmos. Chem. Phys.* **2017**, *17* (9), 5583–5599.
- (45) Triesch, N.; van Pinxteren, M.; Engel, A.; Herrmann, H. Concerted measurements of free amino acids at the Cabo Verde islands: high enrichments in submicron sea spray aerosol particles and cloud droplets. *Atmos. Chem. Phys.* **2021**, *21* (1), 163–181.
- (46) Scalabrin, E.; Zangrando, R.; Barbaro, E.; Kehrwald, N. M.; Gabrieli, J.; Barbante, C.; Gambaro, A. Amino acids in Arctic aerosols. *Atmos. Chem. Phys.* **2012**, *12* (21), 10453–10463.
- (47) Ault, A. P.; Moffet, R. C.; Baltrusaitis, J.; Collins, D. B.; Ruppel, M. J.; Cuadra-Rodriguez, L. A.; Zhao, D.; Guasco, T. L.; Ebben, C. J.; Geiger, F. M.; Bertram, T. H.; Prather, K. A.; Grassian, V. H. Size-dependent changes in sea spray aerosol composition and properties

- with different seawater conditions. Environ. Sci. Technol. 2013, 47 (11), 5603-12.
- (48) Marcolli, C.; Krieger, U. K. Phase changes during hygroscopic cycles of mixed organic/inorganic model systems of tropospheric aerosols. *J. Phys. Chem. A* **2006**, *110* (5), 1881–93.
- (49) Verdugo, P.; Alldredge, A. L.; Azam, F.; Kirchman, D. L.; Passow, U.; Santschi, P. H. The oceanic gel phase: a bridge in the DOM-POM continuum. *Mar. Chem.* **2004**, 92 (1–4), 67–85.
- (50) Xu, H. C.; Lv, H.; Liu, X.; Wang, P. F.; Jiang, H. L. Electrolyte Cations Binding with Extracellular Polymeric Substances Enhanced Microcystis Aggregation: Implication for Microcystis Bloom Formation in Eutrophic Freshwater Lakes. *Environ. Sci. Technol.* **2016**, *50* (17), 9034–9043.
- (51) Lee, C. P.; Riva, M.; Wang, D.; Tomaz, S.; Li, D.; Perrier, S.; Slowik, J. G.; Bourgain, F.; Schmale, J.; Prevot, A. S. H.; Baltensperger, U.; George, C.; El Haddad, I. Online Aerosol Chemical Characterization by Extractive Electrospray Ionization-Ultrahigh-Resolution Mass Spectrometry (EESI-Orbitrap). *Environ. Sci. Technol.* **2020**, *54* (7), 3871–3880.
- (52) Perraud, V.; Bruns, E. A.; Ezell, M. J.; Johnson, S. N.; Yu, Y.; Alexander, M. L.; Zelenyuk, A.; Imre, D.; Chang, W. L.; Dabdub, D.; Pankow, J. F.; Finlayson-Pitts, B. J. Nonequilibrium atmospheric secondary organic aerosol formation and growth. *Proc. Natl. Acad. Sci. U. S. A.* 2012, 109 (8), 2836–41.
- (53) Rothfuss, N. E.; Petters, M. D. Characterization of the temperature and humidity-dependent phase diagram of amorphous nanoscale organic aerosols. *Phys. Chem. Chem. Phys.* **2017**, *19* (9), 6532–6545.
- (54) Riva, M.; Heikkinen, L.; Bell, D. M.; Peräkylä, O.; Zha, Q.; Schallhart, S.; Rissanen, M. P.; Imre, D.; Petäjä, T.; Thornton, J. A.; Zelenyuk, A.; Ehn, M. Chemical transformations in monoterpenederived organic aerosol enhanced by inorganic composition. *npj Clim. Atmos. Sci.* **2019**, 2 (1), 2.
- (55) Li, Y.; Day, D. A.; Stark, H.; Jimenez, J. L.; Shiraiwa, M. Predictions of the glass transition temperature and viscosity of organic aerosols from volatility distributions. *Atmos. Chem. Phys.* **2020**, *20* (13), 8103–8122.
- (56) Juttner, F. Liberation of 5,8,11,14,17-Eicosapentaenoic Acid and Other Polyunsaturated Fatty Acids from Lipids as a Grazer Defense Reaction in Epilthic Diatom Biofilms. *J. Phycol.* **2001**, *37* (5), 744–755.
- (57) Verity, P. G.; Smayda, T. J.; Sakshaug, E. Photosynthesis, excretion, and growth rates of Phaeocystis colonies and solitary cells. *Polar Res.* **1991**, *10* (1), 117–128.
- (58) Passow, U. Transparent exopolymer particles (TEP) in aquatic environments-annotated. *Prog. Oceanogr.* **2002**, *55*, 287–333.
- (59) Zhu, Y.; Chen, P.; Bao, Y.; Men, Y.; Zeng, Y.; Yang, J.; Sun, J.; Sun, Y. Complete genome sequence and transcriptomic analysis of a novel marine strain Bacillus weihaiensis reveals the mechanism of brown algae degradation. *Sci. Rep.* **2016**, *6*, 38248.
- (60) Mikhailov, E.; Vlasenko, S.; Rose, D.; Poschl, U. Mass-based hygroscopicity parameter interaction model and measurement of atmospheric aerosol water uptake. *Atmos. Chem. Phys.* **2013**, *13* (2), 717–740.
- (61) Shiraiwa, M.; Zuend, A.; Bertram, A. K.; Seinfeld, J. H. Gasparticle partitioning of atmospheric aerosols: interplay of physical state, non-ideal mixing and morphology. *Phys. Chem. Chem. Phys.* **2013**, *15* (27), 11441–53.
- (62) Wolf, M. J.; Zhang, Y.; Zawadowicz, M. A.; Goodell, M.; Froyd, K.; Freney, E.; Sellegri, K.; Rosch, M.; Cui, T.; Winter, M.; Lacher, L.; Axisa, D.; DeMott, P. J.; Levin, E. J. T.; Gute, E.; Abbatt, J.; Koss, A.; Kroll, J. H.; Surratt, J. D.; Cziczo, D. J. A biogenic secondary organic aerosol source of cirrus ice nucleating particles. *Nat. Commun.* **2020**, *11* (1), 4834.
- (63) Berkemeier, T.; Shiraiwa, M.; Pöschl, U.; Koop, T. Competition between water uptake and ice nucleation by glassy organic aerosol particles. *Atmos. Chem. Phys.* **2014**, *14* (22), 12513–12531.

- (64) Murray, B. J.; Wilson, T. W.; Dobbie, S.; Cui, Z.; Al-Jumur, S. M. R. K.; Möhler, O.; Schnaiter, M.; Wagner, R.; Benz, S.; Niemand, M.; Saathoff, H.; Ebert, V.; Wagner, S.; Kärcher, B. Heterogeneous nucleation of ice particles on glassy aerosols under cirrus conditions. *Nat. Geosci.* **2010**, 3 (4), 233–237.
- (65) Wilson, T. W.; Murray, B. J.; Wagner, R.; Möhler, O.; Saathoff, H.; Schnaiter, M.; Skrotzki, J.; Price, H. C.; Malkin, T. L.; Dobbie, S.; Al-Jumur, S. M. R. K. Glassy aerosols with a range of compositions nucleate ice heterogeneously at cirrus temperatures. *Atmos. Chem. Phys.* **2012**, *12* (18), 8611–8632.
- (66) Schill, G. P.; Tolbert, M. A. Heterogeneous Ice Nucleation on Simulated Sea-Spray Aerosol Using Raman Microscopy. *J. Phys. Chem.* C **2014**, *118* (50), 29234–29241.
- (67) Koreiviene, J.; Anne, O.; Kasperoviciene, J.; Burskyte, V. Cyanotoxin management and human health risk mitigation in recreational waters. *Environ. Monit. Assess.* **2014**, *186* (7), 4443–59.
- (68) Van Dolah, F. M. Marine Algal Toxins: Origins, Health Effects, and Their Increased Occurance. *Environ. Health Perspect.* **2000**, *108*, 133–141.
- (69) Carmichael, W. W. Health Effects of Toxin-Producing Cyanobacteria: "The CyanoHABs. *Hum. Ecol. Risk Assess.* **2001**, 7 (5), 1393–1407.
- (70) Kite-Powell, H. L.; Fleming, L. E.; Backer, L. C.; Faustman, E. M.; Hoagland, P.; Tsuchiya, A.; Younglove, L. R.; Wilcox, B. A.; Gast, R. J. Linking the oceans to public health: current efforts and future directions. *Environ. Health* **2008**, 7 (Suppl. 2), S6.
- (71) Huot, Y.; Babin, M.; Bruyant, F.; Grob, C.; Twardowski, M. S.; Claustre, H. Relationship between phyotsynthetic parameters and different proxies of phytoplankton biomass in the subtropical ocean. *Biogeosciences* **2007**, *4*, 853–868.
- (72) Virtanen, A.; Joutsensaari, J.; Koop, T.; Kannosto, J.; Yli-Pirila, P.; Leskinen, J.; Makela, J. M.; Holopainen, J. K.; Poschl, U.; Kulmala, M.; Worsnop, D. R.; Laaksonen, A. An amorphous solid state of biogenic secondary organic aerosol particles. *Nature* **2010**, 467 (7317), 824–7.
- (73) Jain, S.; Petrucci, G. A. A New Method to Measure Aerosol Particle Bounce Using a Cascade Electrical Low Pressure Impactor. *Aerosol Sci. Technol.* **2015**, 49 (6), 390–399.
- (74) Marjamäki, M.; Lemmetty, M.; Keskinen, J. ELPI Response and Data Reduction I: Response Functions. *Aerosol Sci. Technol.* **2005**, *39* (7), 575–582.
- (75) Jarvinen, A.; Aitomaa, M.; Rostedt, A.; Keskinen, J.; Yli-Ojanpera, J. Calibration of the new electrical low pressure impactor (ELPI plus). *J. Aerosol Sci.* **2014**, *69*, 150–159.
- (76) Maricq, M. M.; Podsiadlik, D. H.; Chase, R. E. Size distributions of motor vehicle exhaust PM: a comparison between ELPI and SMPS measurements. *Aerosol Sci. Technol.* **2000**, 33, 239–260.
- (77) Price, H. D.; Stahlmecke, B.; Arthur, R.; Kaminski, H.; Lindermann, J.; Dauber, E.; Asbach, C.; Kuhlbusch, T. A. J.; BeruBe, K. A.; Jones, T. P. Comparison of instruments for particle number size distribution measurements in air quality monitoring. *J. Aerosol Sci.* **2014**, *76*, 48–55.
- (78) Ristimaki, J.; Virtanen, A.; Marjamaki, M.; Rostedt, A.; Keskinen, J. On-line measurement of size distribution and effective density of submicron aerosol particles. *J. Aerosol Sci.* **2002**, 33 (11), 1541–1557.
- (79) Kannosto, J.; Yli-Pirila, P.; Hao, L.-Q.; Leskinen, J.; Jokiniemi, J.; Makela, J. M.; Joutsensaari, J.; Laaksonen, A.; Worsnop, D. R.; Keskinen, J.; Virtanen, A. Bounce characteristics of α -pinene-derived soa particles with implications to physical phase. *Boreal Environ. Res.* **2012**, *18*, 329–340.
- (80) Kidd, C.; Perraud, V.; Wingen, L. M.; Finlayson-Pitts, B. J. Integrating phase and composition of secondary organic aerosol from the ozonolysis of alpha-pinene. *Proc. Natl. Acad. Sci. U. S. A.* **2014**, *111* (21), 7552–7.
- (81) Saukko, E.; Lambe, A. T.; Massoli, P.; Koop, T.; Wright, J. P.; Croasdale, D. R.; Pedernera, D. A.; Onasch, T. B.; Laaksonen, A.; Davidovits, P.; Worsnop, D. R.; Virtanen, A. Humidity-dependent

- phase state of SOA particles from biogenic and anthropogenic precursors. *Atmos. Chem. Phys.* **2012**, *12* (16), 7517–7529.
- (82) Power, R. M.; Simpson, S. H.; Reid, J. P.; Hudson, A. J. The transition from liquid to solid-like behaviour in ultrahigh viscosity aerosol particles. *Chem. Sci.* **2013**, *4* (6), 2597–2604.
- (83) Maricq, M. M.; Xu, N.; Chase, R. E. Measuring Particulate Mass Emissions with the Electrical Low Pressure Impactor. *Aerosol Sci. Technol.* **2006**, *40* (1), 68–79.
- (84) Lopez-Hilfiker, F. D.; Pospisilova, V.; Huang, W.; Kalberer, M.; Mohr, C.; Stefenelli, G.; Thornton, J. A.; Baltensperger, U.; Prevot, A. S. H.; Slowik, J. G. An extractive electrospray ionization time-of-flight mass spectrometer (EESI-TOF) for online measurement of atmospheric aerosol particles. *Atmos. Meas. Tech.* **2019**, *12* (9), 4867–4886.
- (85) Doezema, L. A.; Longin, T.; Cody, W.; Perraud, V.; Dawson, M. L.; Ezell, M. J.; Greaves, J.; Johnson, K. R.; Finlayson-Pitts, B. J. Analysis of secondary organic aerosols in air using extractive electrospray ionization mass spectrometry (EESI-MS). *RSC Adv.* **2012**, *2* (7), 2930–2938.
- (86) Qi, L.; Chen, M.; Stefenelli, G.; Pospisilova, V.; Tong, Y.; Bertrand, A.; Hueglin, C.; Ge, X.; Baltensperger, U.; Prévôt, A. S. H.; Slowik, J. G. Organic aerosol source apportionment in Zurich using an extractive electrospray ionization time-of-flight mass spectrometer (EESI-TOF-MS) Part 2: Biomass burning influences in winter. *Atmos. Chem. Phys.* **2019**, *19* (12), 8037–8062.
- (87) Gu, H.; Xu, N.; Chen, H. Direct analysis of biological samples using extractive electrospray ionization mass spectrometry (EESI-MS). *Anal. Bioanal. Chem.* **2012**, *403* (8), 2145–53.
- (88) Stark, H.; Yatavelli, R. L. N.; Thompson, S. L.; Kimmel, J. R.; Cubison, M. J.; Chhabra, P. S.; Canagaratna, M. R.; Jayne, J. T.; Worsnop, D. R.; Jimenez, J. L. Methods to extract molecular and bulk chemical information from series of complex mass spectra with limited mass resolution. *Int. J. Mass Spectrom.* **2015**, *389*, 26–38.
- (89) Canagaratna, M. R.; Jimenez, J. L.; Kroll, J. H.; Chen, Q.; Kessler, S. H.; Massoli, P.; Hildebrandt Ruiz, L.; Fortner, E.; Williams, L. R.; Wilson, K. R.; Surratt, J. D.; Donahue, N. M.; Jayne, J. T.; Worsnop, D. R. Elemental ratio measurements of organic compounds using aerosol mass spectrometry: characterization, improved calibration, and implications. *Atmos. Chem. Phys.* **2015**, *15* (1), 253–272.
- (90) Jimenez, J. L.; et al. Ambient aerosol sampling using the Aerodyne Aerosol Mass Spectrometer. J. Geophys. Res. 2003, 108 (D7), 8425.